Langmuir

Article

pubs.acs.org/Langmuir

Tethered Poly(2-isopropyl-2-oxazoline) Chains: Temperature Effects on Layer Structure and Interactions Probed by AFM Experiments and Modeling

Junxue An,[†] Xiaoyan Liu,[†] Per Linse,[‡] Andra Dėdinaitė,[†,§] Françoise M. Winnik,[∥,⊥] and Per M. Claesson*[,†,§]

[†]School of Chemical Science and Engineering, Department of Chemistry, Division of Surface and Corrosion Science, KTH Royal Institute of Technology, Drottning Kristinas väg 51, SE-100 44 Stockholm, Sweden

[‡]Physical Chemistry, Department of Chemistry, Lund University, Box 124, SE-221 00 Lund, Sweden

[§]Chemistry, Materials and Surfaces, SP Technical Research Institute of Sweden, Box 5607, SE-114 86 Stockholm, Sweden

[∥]Department of Chemistry and Faculty of Pharmacy, University of Montreal, CP 6128 Succursale Centre Ville, Montreal, QC H3C 3J7, Canada

[⊥]National Institute for Materials Science, WPI International Center for Materials Nanoarchitectonics (MANA), 1-1 Namiki, Tsukuba, Ibaraki 305-0044, Japan

Supporting Information

ABSTRACT: Thermoresponsive polymer layers on silica surfaces have been obtained by utilizing electrostatically driven adsorption of a cationic−nonionic diblock copolymer. The cationic block provides strong anchoring to the surface for the nonionic block of poly(2-isopropyl-2-oxazoline), referred to as PIPOZ. The PIPOZ chain interacts favorably with water at low temperatures, but above 46 °C aqueous solutions of PIPOZ phase separate as water becomes a poor solvent for the polymer. We explore how a change in solvent condition affects interactions between such adsorbed layers and report temperature effects on both normal forces and friction forces. To gain further insight, we utilize self-consistent lattice mean-field theory to follow how changes in temperature affect the polymer segment density distributions and to calculate surface force curves. We find that with worsening of the solvent condition an attraction develops between the adsorbed PIPOZ layers, and this observation is in good agreement with predictions of the mean-field theory. The modeling also demonstrates that the segment density profile and the degree of chain interpenetration under a given load between two PIPOZ-coated surfaces rise significantly with increasing temperature.

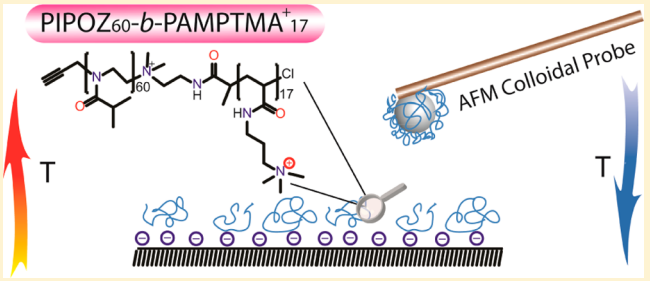

1. INTRODUCTION

Temperature-responsive polymers constitute a subgroup of stimuli-responsive polymers distinguished by significant change in state in response to temperature variations.[1] In most cases, this temperature sensitivity reflects conformational changes of the polymer chains.[2] For most temperature-responsive polymers, water becomes a poorer solvent with increasing temperature, and above a lower critical solution temperature (LCST) the polymer solution phase separates into a polymer rich and a polymer-depleted phase.[1,2] This is the case for polymers like poly(*N*-isopropylacrylamide) (PNIPAAM),[1,3] poly(ethylene oxide) (PEO),[4,5] poly(propylene oxide) (PPO),[6,7] poly(2-(dimethylamino)ethyl methacrylate) (PDMAEMA),[8,9] and poly(2-alkyl-2-oxazoline).[10,11] When attached to a solid support, these polymers can recognize small temperature changes in the solvent and respond by swelling or collapsing, which affects surface properties, such as wettability,[12] adhesion,[13] and lubrication.[14] These effects have become increasingly important for the development of smart devices, and since temperature-responsive polymers offer convenient tuning of surface properties, they have received much attention in, for instance, controlled release and drug delivery,[15] sensors,[16] and cell sheet engineering.[17] One of the best-studied temperature-responsive polymers is PNIPAAM, which has a LCST of about 32 °C in bulk aqueous solution. However, the LCST of PNIPAAM is dependent on molecular weight, polymer concentration, and the presence of end-group functionalities.[18,19] Surfaces bearing PNIPAAM chains have also been widely investigated[13,20−22] for their temperature-dependent surface properties.

Poly(2-isopropyl-2-oxazoline), a structural isomer of PNIPAAM, exhibits a LCST around 45 °C in aqueous solution,

Received: November 28, 2014
Revised: February 9, 2015
Published: February 16, 2015

DOI: 10.1021/la504653w
Langmuir 2015, 31, 3039−3048

depending on polymer molecular weight and solution concentration,[23,24] yet there are only a few studies concerned with the properties of PIPOZ on surfaces. Among these, Rehfeldt et al. studied the static and dynamic swelling of grafted poly(2-alkyl-2-oxazoline) films on silicon/silicon dioxide substrates by water vapor. They discovered that both the static and dynamic swelling depend on the chain length, and they regarded the PIPOZ layer as being a promising candidate for the fabrication of tethered lipid bilayers with polymer spacers.[25] Konradi et al. studied the protein-repellent properties of a poly(2-methyl-2-oxazoline) (PMOXA)-based coating by exposing the formed monolayers to full human serum. They found that the PMOXA-based coating with an optimal side-chain grafting density could eliminate protein adsorption to a level of <2 ng/cm^2, which is as good as the best poly(ethylene glycol)-based coatings.[26] In another study, PIPOZ was used to modify macroscopic surfaces by the grafting-to method. These PIPOZ-grafted surfaces were then used to immobilize gold nanoparticles, demonstrating potentials in sensing, biomedical, and catalytic applications.[27] Our group studied interfacial properties of electrostatically anchored PIPOZ layers on silica substrates, particularly how the film thickness and water content varied in the temperature range from 25 to 45 °C, and observed a significant adsorption hysteresis during heating−cooling cycles.[28] Very recently, a review article extensively describing poly(2-oxazoline)s as materials for biomedical applications has appeared.[29] However, to our knowledge no investigation on interactions between surfaces coated with PIPOZ chains and their nanotribological properties has been reported so far.

In this study we have experimentally determined the interactions between layers formed by adsorption of a diblock copolymer, containing one charged block and one uncharged PIPOZ block, on silica surfaces. We utilize the atomic force microscopy (AFM) colloidal probe technique to investigate surface forces and friction force, covering the temperature range 25 to 50 °C. This allows us to explore both good and poor solvent conditions for the PIPOZ chain. To gain further insight, we also performed theoretical modeling, utilizing self-consistent lattice mean-field calculations, which previously has been utilized for analyzing adsorption properties of charged−uncharged diblock copolymers[30,31] and temperature-responsive properties of grafted polymer layers.[32] The modeling results are found to agree well with experiments and delivers insight into temperature-induced changes in segment density profiles, surface interactions, and interpenetration of opposing polymer layers under load.

2. MATERIALS AND METHODS

2.1. Materials. Poly(2-isopropyl-2-oxazoline)$_{60}$-*b*-poly(3-acrylamidopropylmethylammonium)$_{17}$ (PIPOZ$_{60}$-*b*-PAMPTMA$_{17}$) was prepared as described previously[10] with a molecular weight M_n = 10.3 kDa. This polymer consists of one nonionic thermoresponsive block and one cationic block (see Figure 1). The PIPOZ block has a molecular weight M_n = 7.0 kDa and a mass polydispersity M_w/M_n = 1.06 as determined by GPC.[10] The cationic block, PAMPTMA, contains one charge per repeat unit, and the average number of charged units per copolymer was determined to be ≈17 by ^{1}H NMR spectroscopy. The phase transition temperature of this diblock copolymer is 46.1 °C at the polymer concentration 1.0 g/L.[10]

Poly(2-isopropyl-2-oxazoline) is a crystalline polymer with a melting temperature ∼200 °C.[33] Amorphous PIPOZ is recovered after cationic ring-opening polymerization of 2-isopropyl-2-oxazoline. It readily dissolves in water at room temperature or below. However, when an aqueous PIPOZ solution is heated at ∼65 °C for a few hours, PIPOZ crystallizes, yielding a semicrystalline material that is insoluble in water at all temperature.[34,35]

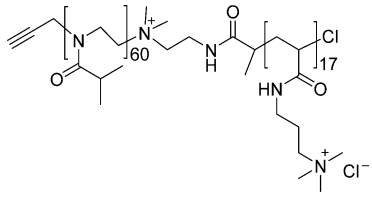

Figure 1. Chemical structure of poly(2-isopropyl-2-oxazoline)$_{60}$-*b*-poly(3-acrylamidopropyltrimethylammonium)$_{17}$, abbreviated as PIPOZ$_{60}$-*b*-PAMPTMA$_{17}$.

Sodium chloride (NaCl, BioXtra, ≥99.5%) was purchased from Sigma-Aldrich and used as received. Water was pretreated with a Milli-RO 10 plus unit and further purified with a Milli-Q PLUS 185 system. The resistivity after the treatment was 18 MΩ cm, and the total organic carbon content of the water did not exceed 2 ppb.

Stock solutions of 500 ppm were prepared by dissolving PIPOZ$_{60}$-*b*-PAMPTMA$_{17}$ in 0.1 mM NaCl aqueous solution under stirring and then diluting this solution with 0.1 mM NaCl to 100 ppm. The pH of the solutions was measured with a pH meter (PHM 210, Meterlab) and adjusted by adding small amounts of NaOH (1 M) and HCl (0.6 M) solutions to achieve pH 9.

2.2. Atomic Force Microscope (AFM) with Colloidal Probe. A Nanoscope Multimode 8 Pico Force AFM (Bruker) was employed for normal and friction force measurements that were performed in a fused silica liquid cell (cell volume ≈0.1 mL, MTFML, Bruker). A spherical silica particle with a diameter of ≈7 μm (G. Kisker GmbH) was attached to the end of the cantilever with the aid of an Ependorf Micromanipulator 5171, a Nikon Optiphot 100S reflection microscope, and a small amount of epoxy glue (Araldite, Switzerland). The size of the particles was determined using a Nicon Optiphot 100S reflection microscope, employing image analysis with National Instrument Vision Assistant 8.0. Rectangular tipless cantilevers (MikroMasch, CSC12/tipless/Cr−Au) ≈250 μm long and 35 μm wide with normal spring constants in the range 0.02−0.2 N/m were chosen for all normal and friction force measurements. The values of the normal (k_N) and the torsional (k_φ) spring constants for each cantilever were determined using the AFM Tune IT v2.5 software (Force IT, Sweden) adopting a method based on thermal noise with hydrodynamic damping.[36,37] The spring constants were determined before attaching the silica particle. The lateral photodetector sensitivity (δ, V/rad) was calibrated using the method of tilting the AFM head.[38]

2.3. Experimental Procedure. The fused silica cell and all other tools were cleaned by immersion in 2% Hellmanex (Hellma GmbH) solution for 1 h and then rinsed excessively with Milli-Q water. The cells were then rinsed with ethanol before being dried with a stream of filtered nitrogen gas. The AFM experiment was started by measuring normal and friction forces between a silica colloidal probe and a flat silica surface (Wafernet, Germany) across a 0.1 mM NaCl solution at pH 9. The silica surfaces are negatively charged due to dissociation of some of the surface silanol groups, and the surface charge density varies depending on pH, ionic strength, and cleaning procedure.[39] Next, a 100 ppm PIPOZ$_{60}$-*b*-PAMPTAM$_{17}$ solution in 0.1 mM NaCl of pH 9 was injected into the fluid cell, and the adsorption was allowed to proceed for 1 h, which is sufficient for reaching adsorption equilibrium,[28] after which the polymer solution was replaced by 0.1 mM NaCl of pH 9. Normal and friction forces were measured between such preadsorbed polymer layers at 25 °C, and then the temperature was increased in steps of 5 °C until it reached the maximum temperature, 45 °C, which was followed by a cooling process from 45 to 25 °C in steps of 5 °C. After reaching the intended temperature, 40 min was allowed for the polymer layers to reach equilibrium before performing the normal and friction force measurements. Finally, the temperature was increased from 25 to 50 °C directly, and force measurements were performed at 50 °C.

DOI: 10.1021/la504653w
Langmuir 2015, 31, 3039−3048

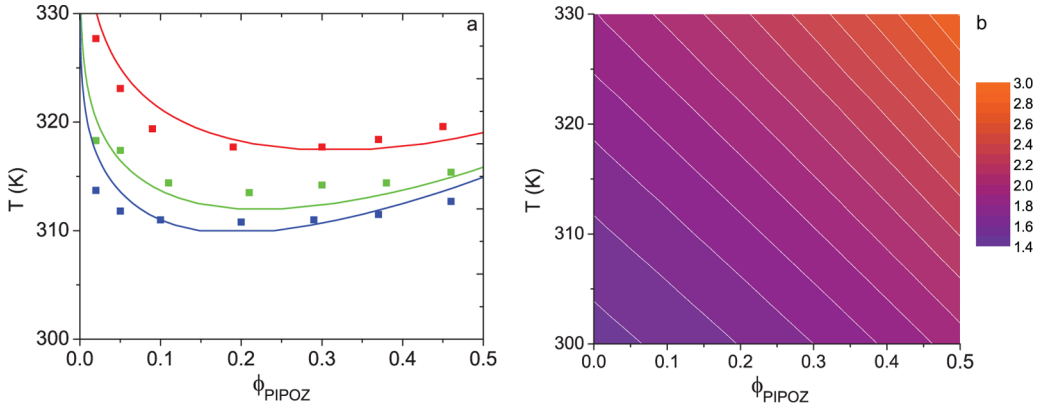

Figure 2. (a) Experimental binodal curves (symbols) for the binary water−PIPOZ solution for PIPOZ molecular mass 3 kDa (red), 6 kDa (green), and 8 kDa (blue)[45] and corresponding calculated binodal curves for r_{PIPOZ} = 29 (red), 55 (green), and 70 (blue). (b) Calculated effective water−PIPOZ interaction $RT\chi_{water,PIPOZ}$ (in kJ/mol) as a function of the PIPOZ volume fraction ϕ_{PIPOZ} and temperature T. Equidistant curves are given for $RT\chi_{water,PIPOZ}$ = 1.5, 1.6, ..., 2.7 kJ/mol.

2.4. Theoretical Model. The measured normal forces of the experimental systems were modeled using a lattice mean-field theory. The theory was initially developed by Scheutjens and Fleer[40,41] and later extended, among others, by Linse and Björling[42] to enable modeling of thermoresponsive polymers following ideas proposed by Karlström.[43] After its development, the theory has successfully been applied to PEO, PPO, and PNIPAAM containing aqueous solution.[32,44] A brief description of the theory is given in the Supporting Information.

Within the framework of the lattice mean-field theory, we have constructed a model system adapted to our experimental set up by applying the following conditions:

I. Planar Surfaces. The experimentally observed normal force between one flat and one spherical surface can be related to the potential energy between two planar surfaces through the Derjaugin approximation valid for interactions of shorter range than the spherical curvature.

II. Uncharged Surfaces. The long-range Coulomb repulsion between the surfaces is *not* modeled, since (1) our focus is on the thermoresponse of the polymer and (2) the Coulomb repulsion can well be characterized by the Poisson−Boltzmann (PB) theory. Double-layer forces with intervening aqueous solution of monovalently charged species at ambient temperature are accurately described by the PB theory.

III. Polymer-Grafted Surfaces. The layer of irreversibly adsorbed diblock copolymer is modeled by a fixed grafting density of a thermoresponsive homopolymer representing PIPOZ. The grafting density was determined from the experimentally adsorbed amount of diblock polymers.

IV. Polymer-Free Solution. According to the experimental protocol.

In the current application, PIPOZ is represented by a chain consisting of r_{PIPOZ} = 62 segments, each representing a PIPOZ monomer. The chains are grafted onto a smooth surface with the grafting density σ (number of chains per lattice length squared). The values of the parameters describing (i) the two states of a PIPOZ segment and (ii) the interactions in the binary water−PIPOZ solution were here determined by fitting theoretical binodal curves to experimental ones for three molecular masses of PIPOZ. The effective water−PIPOZ interaction parameter $\chi_{water,PIPOZ}$ (corresponding to the Flory interaction parameter[44]) becomes a weighted average of $\chi_{water,PIPOZp}$ and $\chi_{water,PIPOZap}$, characterizing the interaction between water and PIPOZ in the polar and apolar state, respectively. Their weights are determined by free energy minimization.[42]

The experimental[45] and fitted binodal curves are displayed in Figure 2a, and the obtained values are given in Table 1. Overall, the fit is satisfactorily provided by the simple theory and the use of a monodisperse representation of the polydisperse PIPOZ mass distribution. Additional comments on the fit are given in the Supporting Information. The effective water−PIPOZ interaction $RT\chi_{water,PIPOZ}$ as a function of the PIPOZ volume fraction and temperature is given in Figure 2b. We observe an increase of $\chi_{water,PIPOZ}$ with increasing temperature, motivating the term "thermo-responsive". Moreover, the polymer also becomes more hydrophobic at increasing polymer volume fraction, as more polymer and fewer water contacts favor the hydrophobic state. Hence, not only the temperature but also the solution composition affects the hydrophobic−hydrophilic balance of PIPOZ.

Table 1. Model Parameters

internal state parameter of IPOZ[a]			
species	state	U_{AB} (kJ/mol)	g_{AB}
IPOZ	polar	0	1
	apolar	18.4[b]	1095[b]
interaction parameters $RT\chi$ (kJ/mol)[a]			
	water	$PIPOZ_p$	$PIPOZ_{ap}$	surface
water	–	1.1[b]	7.0[b]	0[c]
$IPOZ_p$	–	–	1.5[b]	0[c]
$IPOZ_{ap}$	–	–	–	0[c]
other parameters of the surface system				
degree of polymerization of PIPOZ	r_{PIPOZ} = 62			
temperature	T/K = 300−325			
size of a lattice cell	d/nm = 0.5			
grafting density[d]	σ = 0.010			
bulk PIPOZ volume fraction	ϕ_{PIPOZ} = 0			
conversion factor[e]	$F/R/(mN/m) = 0.0604A_{int}/LkT$			

[a]Internal state parameters U_{AB} and g_{AB} and the interaction parameter χ are further described in the Supporting Information. [b]Obtained from fit to experimental phase diagrams; see Figure 2. [c]Selected for simplicity. [d]Obtained from experimental adsorption data and the size of a lattice cell (see text). [e]Obtained from the size of a lattice cell.

The fitted parameters given in Table 1 were used in the modeling of the interaction between the two polymer-grafted surfaces. In addition to these parameters, we need to assign interaction parameters for the interaction of water and PIPOZ with the surfaces. If nothing else is stated, we assume an athermal condition, i.e., no preference of any of the two components for the surface. When making contact with the experimental system, a value of the length of a lattice cell has to be assigned; here we have used the reasonable value d = 0.5 nm. Experimentally, a spacing of 4.9 nm between adsorbed diblock polymers at pH = 9 have been obtained,[28] which with d = 0.5 nm becomes converted to 1 polymer grafted per 100 lattice surface sites or the grafting density σ = 0.010. Finally, for a polymer with r segments we notice that $2(r_{PIPOZ})^{\alpha}\sigma^{1/2} \approx 1$ for $\alpha \approx 0.5$−0.6 depending on solvent condition, implying that neighboring polymers grafted on the

DOI: 10.1021/la504653w
Langmuir 2015, 31, 3039−3048

same surface are weakly interacting with each other, and hence they do not form a proper polymer brush.

3. RESULTS AND DISCUSSION

Experimental normal and friction forces at different temperatures will now be reported and followed by lattice mean-field calculations providing complementary results on normal forces and polymer distributions.

3.1. Experimental Observations. Before presenting our results on normal and friction forces, we describe some essential features of the solution and adsorption properties of $PIPOZ_{60}$-*b*-$PAMPTAM_{17}$ as reported in previous publications. $PIPOZ_{60}$-*b*-$PAMPTAM_{17}$ is highly soluble in water at room temperature; however, water progressively becomes a worse solvent for $PIPOZ_{60}$-*b*-$PAMPTAM_{17}$ as the temperature increases. The temperature responsive block, $PIPOZ_{60}$, has a phase transition temperature of 47 °C,[10] but the dehydration of the amide groups in the PIPOZ homopolymer occurs gradually from 20 °C.[35] A gradual reduction in the water content of adsorbed layers of $PIPOZ_{60}$-*b*-$PAMPTAM_{17}$ has also been reported.[28] The phase transition temperature of $PIPOZ_{60}$-*b*-$PAMPTAM_{17}$ is 46 °C.[10]

Below the phase transition temperature a monolayer of $PIPOZ_{60}$-*b*-$PAMPTAM_{17}$ adsorbs to silica surfaces, and above this value deposition of aggregates have been reported.[28] The mass of the adsorbed $PIPOZ_{60}$-*b*-$PAMPTAM_{17}$ layer at 25 °C, including associated water, is 4.9 mg/m^2, and the water content is about 85%. The surface excess determined by ellipsometry was found to be 0.73 mg/m^2, corresponding to an area per adsorbed chain of about 23.4 nm^2, and the layer thickness was estimated to be about 5 nm.[28]

3.1.1. Normal Forces. The forces measured between two silica surfaces carrying an adsorbed layer of $PIPOZ_{60}$-*b*-$PAMPTMA_{17}$ across a 0.1 mM NaCl (pH 9) solution containing 100 ppm of the polymer are shown in Figure 3.

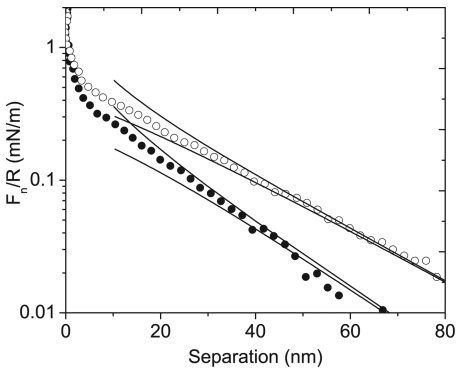

Figure 3. Forces measured on approach between silica surfaces coated with $PIPOZ_{60}$-*b*-$PAMPTMA_{17}$ across 0.1 mM NaCl (pH 9) containing 100 ppm of polymer (filled circles) and after rinsing (open circles). Double-layer forces at constant charge (upper solid curves) and at constant potential (lower solid curves) conditions are also shown.

The long-range interaction is a double-layer force, and this force is characterized by a magnitude of the double-layer potential of 31 mV, a surface charge density of 1.3 mC/m^2, and a Debye length of 18 nm. At surface−surface separations shorter than ≈5 nm, the measured force becomes significantly steeper due to predominance of steric interactions.

Replacement of the polymer-containing solution with 0.1 mM NaCl (pH 9) results in an increase in the range of the double-layer force, which now is characterized by a magnitude of the double-layer potential of 44 mV, a surface charge density of 1.6 mC/m^2, and a Debye length of 21 nm. The measured Debye length is shorter than the 30 nm expected for a 0.1 mM NaCl solution, which is due to addition of NaOH and HCl during adjustment of the solution pH. The observation that the Debye length increases when the charged diblock copolymer is removed from the solution demonstrates that the polyelectrolyte with associated counterions, when present in solution, contribute to the screening of the double-layer force. Moreover, the sign of the double-layer potential cannot be determined from force measurements, and thus from these measurements we cannot determine if adsorption of $PIPOZ_{60}$-*b*-$PAMPTMA_{17}$ overcompensates or undercompensates the surface charge density. However, we note that during rinsing no additional polymer will adsorb, but some polymer may desorb. Nevertheless, since the surface charge density is slightly higher after rinsing (1.6 mC/m^2 compared to 1.3 mC/m^2 prior to rinsing), we reach the conclusion that after rinsing the negative surface charge density is slightly undercompensated by the adsorbed cationic diblock polyelectrolyte (the small excess charge density corresponds to an area per charge of around 100 nm^2).

The normal forces acting between preadsorbed $PIPOZ_{60}$-*b*-$PAMPTMA_{17}$ layers across 0.1 mM NaCl (pH 9) were determined at different temperatures between 25 and 50 °C (see Figure 4). A double-layer force was observed at all temperatures and the double-layer potential was found to vary in the range of 44−31 mV, corresponding to a surface charge density of 1.6−1.1 mC/m^2 and an area per excess charge of 100−150 nm^2. Thus, even though we do observe a significant double-layer force, the excess charge density remains small throughout the experiment. The most striking feature of the forces reported in Figure 4 is the significant temperature dependence of the surface interactions at small separations that are dominated by interactions between polymer segments.

At 25 °C, the short-range interaction is purely repulsive, and no hysteresis is observed between forces measured on approach and on separation. At 30 °C the forces remain purely repulsive, but the repulsion is slightly larger on approach than on separation. This tendency is amplified at 35 °C, where also a notable force minimum, still on the repulsive side, is noted when the surfaces are separated from contact. The force minimum becomes deeper at 40 °C, and at 45 °C and above the force in the minimum is net attractive. From 45 °C the attractive force component is sufficiently strong to be observed also on approach.

The depth of the force minimum as a function of temperature is shown in Figure 5. Clearly, it increases smoothly with increasing temperature from 30 °C, where it is first noted, up to 50 °C that was the highest temperature investigated. This observation is consistent with water becoming a worse solvent for PIPOZ at increasing temperature, which facilitates development of attractive segment−segment interactions between (and within) the adsorbed layers. We note that when the forces were remeasured at 25 °C after the heating process, ≈8 h after the initial measurement at 25 °C, a small force minimum was observed also at this temperature (see Figure 5). This could be caused by some desorption with time or, alternatively, due to the tendency of PIPOZ chains to crystallize at high temperatures that leads to formation of long-lived trapped states.[35] However, this effect is less significant than that caused by the increased solvent temperature (see Figure 5).

DOI: 10.1021/la504653w
Langmuir 2015, 31, 3039−3048

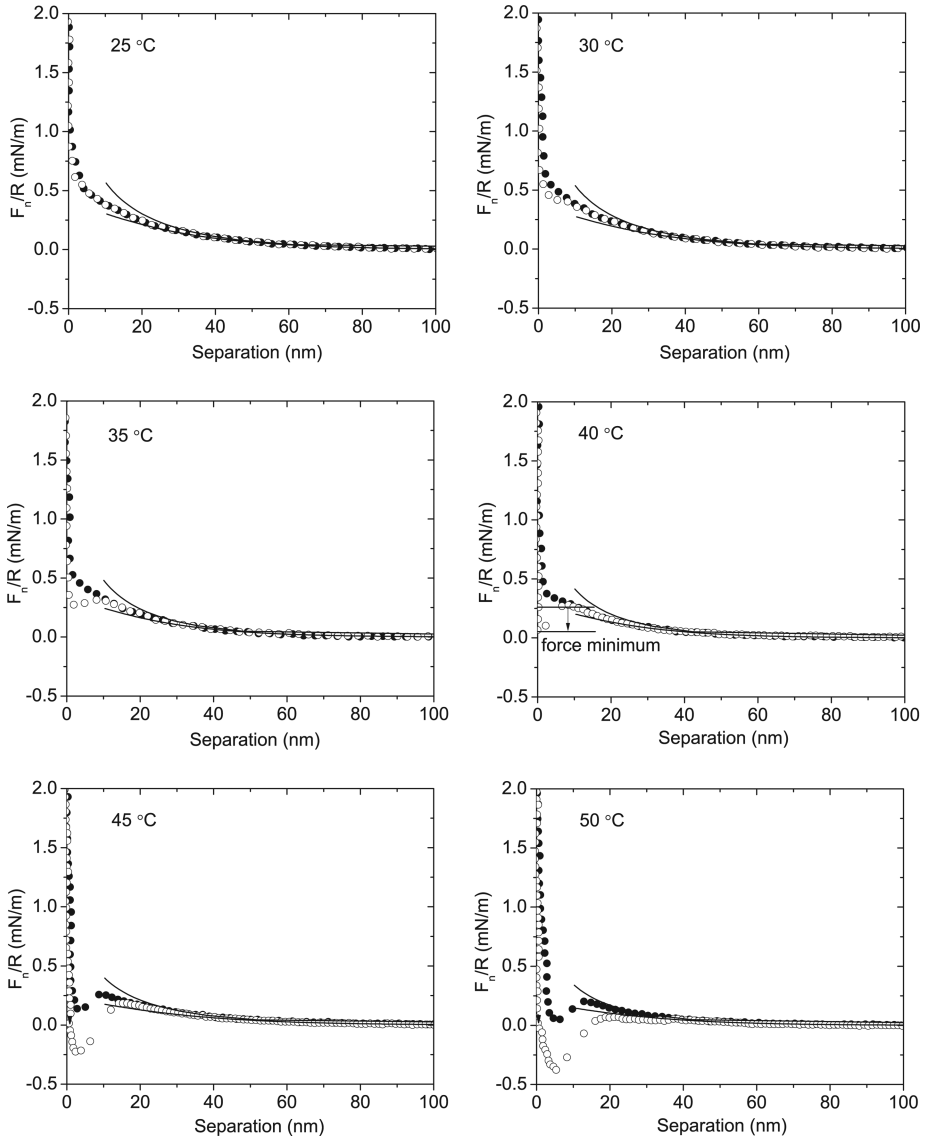

Figure 4. Normal force normalized by radius as a function of separation measured on approach (filled circles) and retraction (open circles) at indicated temperature between silica surfaces coated with PIPOZ$_{60}$-*b*-PAMPTMA$_{17}$ layers across a 0.1 mM NaCl solution at pH 9. Double-layer forces at constant charge (upper solid curves) and at constant potential (lower solid curves) conditions are also shown.

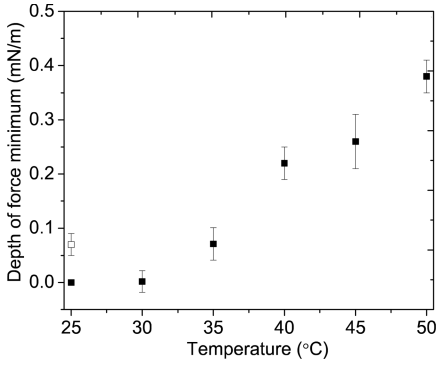

Figure 5. Force minimum depth as a function of temperature (solid symbols) and at 25 °C after cooling, ca. 8 h after the initial measurement at 25 °C (unfilled symbol). The error bars were calculated from 10 force curves.

A reduced solvency with increasing temperature is not unique for PIPOZ but also found for, e.g., PNIPAAM, PDMAEMA, and PEO. It has been observed that the short-range interaction between PEO containing surfactants[46] and polymers[47,48] as well as between surfaces coated with grafted PDMAEMA[8] and adsorbed layers of PNIPAAM chains[14] become more attractive as the temperature increases. However, the magnitude of the change in surface interaction differs significantly. For instance, the change in interaction with temperature is significantly larger for the interaction between surfaces coated with ethyl(hydroxyethyl)cellulose[47] and surfaces carrying electrostatically anchored PNIPAAM chains[14] than observed for PIPOZ in this work. A difference in the temperature dependence of the polymer−water interaction parameter for the different polymers may be the reason for this variation in interaction.

3.1.2. Friction Force. The friction forces measured between silica surfaces coated with a preadsorbed layer of PIPOZ$_{60}$-*b*-PAMPTMA$_{17}$ at different temperatures are shown in Figure 6a. We directly note that Amontons' rule, stating that the friction force should be proportional to the normal load, does not describe our data. At temperatures below 45 °C, the friction

DOI: 10.1021/la504653w
Langmuir 2015, 31, 3039−3048

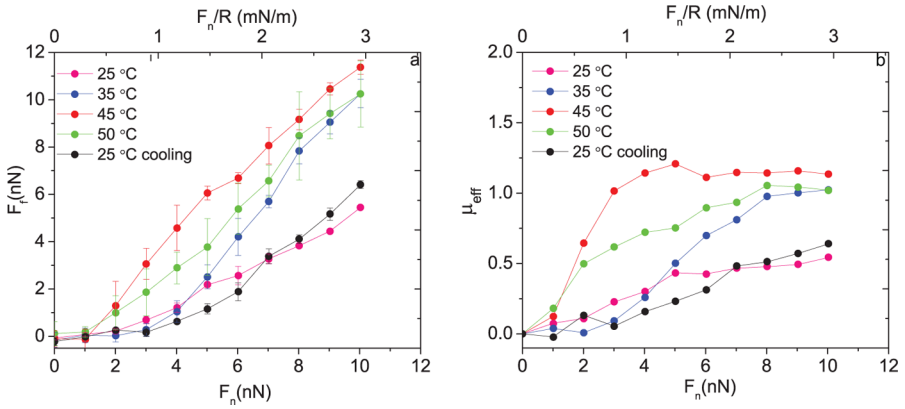

Figure 6. (a) Friction force and (b) effective friction coefficient as a function of applied normal load between silica surfaces carrying a preadsorbed layer of PIPOZ$_{60}$-*b*-PAMPTMA$_{17}$ measured at different temperatures.

force is close to zero at loads below 2 nN, corresponding to F/R < 0.6 mN/m. This is a consequence of the presence of a thick and fluid aqueous layer between the surfaces as long as the double-layer force carries the load (Figure 4). However, once the load exceeds about 2 nN, the friction force reaches a measurable strength. This corresponds to the situation when the two polymer layers are in close contact and a steric force carries the load. As discussed in detail by, e.g., Klein, one important reason for the increase in friction with load is that the interpenetration region between the opposing polymer layers increases and energy dissipation occurs as a consequence of polymer chains being dragged against each other in this region.[49] Similar friction forces were observed on loading and unloading.

Since the frictional force, F_f, is not linearly proportional to the applied load, F_n, it is appropriate to define an effective friction coefficient, μ_{eff}, as

$$\mu_{eff} = \frac{F_f}{F_n} \tag{1}$$

The effective friction coefficient is shown as a function of load for PIPOZ$_{60}$-*b*-PAMPTMA$_{17}$ coated silica surfaces in Figure 6b. The friction force and the effective friction coefficient are similar at 25 and 35 °C as long as the load is below 4 nN. At higher loads a higher friction force is observed at 35 °C. Increasing the temperature further to 45 °C results in significantly higher friction force and effective friction coefficient as soon as the double-layer force no longer carries the load. This is due to the attractive segment−segment interactions that develop as water becomes a poor solvent for the PIPOZ chain. Interestingly, at 50 °C the friction force is lower than at 45 °C. We ascribe this to the tendency of PIPOZ chains to crystallize at high temperatures,[35] and we note that the friction force between crystalline layers has been noted to be less than that between fluid layers of the same molecule.[50,51]

The friction force and the effective friction coefficient at 25 °C observed in the beginning of the experiment and after the temperature cycle are similar, despite that some differences are observed in the normal forces (Figure 5). The highest load used in these experiments, 10 nN, corresponds to a pressure of ≈33 MPa in the nonadhesive case and about 20 MPa at the highest temperature as calculated using JKR theory.[14,52]

The friction forces measured between silica surfaces coated with another diblock copolymer, consisting of a cationic block and a 48 unit long PNIPAAM block, has previously been reported.[14] The friction forces measured below the phase transition temperature for the PNIPAAM-containing diblock copolymer was of similar magnitude compared to what is found for PIPOZ$_{60}$-*b*-PAMPTMA$_{17}$ coated silica surfaces in this study. However, above the phase transition temperature a significantly higher friction was observed for the PNIPAAM-containing diblock copolymer, consistent with the more attractive normal forces observed for this polymer. It is also possible that the tendency of PIPOZ chains to crystallize at higher temperatures contribute to the difference in friction response observed between electrostatically anchored PIPOZ and PNIPAAM layers.

3.2. Model Results. The free energy of the model system, comprising two surfaces each end-grafted with PIPOZ-representing polymers across a water solution, was determined as a function of the surface-to-surface separation using the lattice-mean field theory. The interaction (free) energy between the surfaces A_{int} as a function of their surface separation M is defined as

$$A_{int}(M) = A(M) - A(M \to \infty) \tag{2}$$

where $A(M)$ is the free energy at separation M and $A(M\to\infty)$ the free energy at separations when the surfaces are noninteracting. In the following, the interaction energy is given in the dimensionless unit A_{int}/LkT, where L is the surface area (in lattice units), k the Boltzmann constant, and T the temperature. For convenience, Table 1 provides the relation between the experimental force divided by the surface curvature F/R and the dimensionless interaction energy between the two planar surfaces A_{int}/kTL.

Figure 7 displays the dimensionless interaction energy as a function of the surface sepration for the temerature interval T = 300−325 K. We observe that (i) an attractive minimum M_{min} appears at short separation, (ii) the magnitude of the interaction minimum $A_{int}(M_{min})/LkT$ becomes larger at increasing temperature, and (iii) the location of the minimum M_{min} appears at shorter surface separation at increasing temperature. Observation i originates from the repulsive water−polymer interaction. The mechanism of the model involves a replacement of unfavorable water−polymer contacts by water−water and polymer−polymer contacts, which dominates over the entropic cost appearing at increasing polymer confinment. The mechanism of observation ii is that water−polymer contacts becomes energetically more unfavorable at elevated temerature, which also is the driving force for

DOI: 10.1021/la504653w
Langmuir 2015, 31, 3039−3048

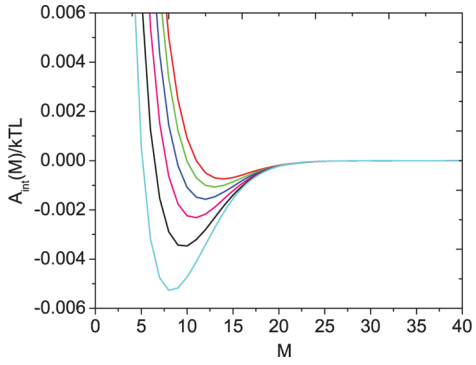

Figure 7. Calculated interaction energy $A_{int}(M)/kTL$ between two planar PIPOZ-grafted surfaces as a function of surface separation M at temperature T = 300, 305, ..., 325 K (top to bottom).

the phase separation shown in Figure 2. Finally, observation iii will be dicussed in conjuction with polymer volume fraction profiles.

Figure 8 shows that the magnitude of the interaction minimum at conditions specificed in Table 1 (red curve)

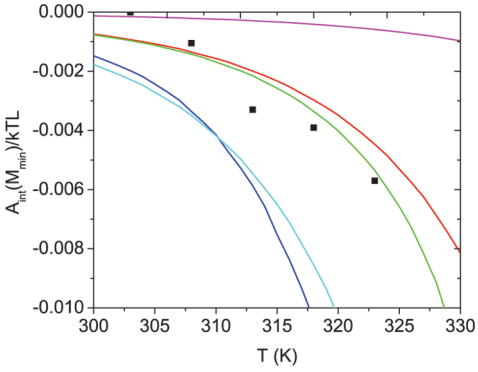

Figure 8. Calculated interaction minimum $A_{int}(M_{min})/kTL$ between two planar PIPOZ-grafted surfaces as a function of the temperature T at conditions specified in Table 1 (red), at grafting densities σ = 0.005 (purple) and 0.015 (light blue), and at the polymer−surface interaction $RT(\chi_{water,PIPOZp}, \chi_{water,PIPOZap})$ = (0, −1) kJ/mol (green) and (−1, −1) kJ/mol (dark blue). The depth of the experimental force minimum, expressed as $A_{int}(M_{min})/kTL$ using the conversion factor given in Table 1, is also given (symbols).

increases 10-fold over 25 K increase of the temperature. The naure of this dependence is strikinly similar to the experimental one given in Figure 5, and these results are discussed in the following section.

At this stage we will also employ our model to examine how the magnitude of the interaction minimum at different temperatures are affected by a variation of the value of the grafting density σ and the surface−polymer interaction parameter $\Delta\chi_{polymer}$. Corresponding data at the grafting densities σ = 0.005 and 0.015 are also included in Figure 8. The principal behavior of a larger magnitude of the interaction minimum at increasing temperature remains also at these grafting densities. Furthermore, the magnitude of the interaction minimum increases strongly with the grafting density, consistent with a grafting density below that of a polymer brush. In the brush limit, the free energy curves are expected to be at most weakly dependent on the grafting density. Figure 8 also displays the dependence of the attractrive polymer−surface interactions $(\Delta\chi_{PIPOZp}, \Delta\chi_{PIPOZap})RT$ = (0, −1) and (−1, −1) kJ/mol. An attractive interaction leads to a deeper interaction minimum and a stronger temperature dependence. Furthermore, the influence of the interaction parameter of the polar state is stronger—the reason being that the fraction of segments in the polar state is larger. Investigation of the polymer profiles reveals mainly changes of the profiles near the surface upon variation of $\Delta\chi_{PIPOZp}$ and $\Delta\chi_{PIPOZap}$.

Figure 9 displays the polymer volume fraction across the solution at the temeperatures T = 300 and 325 K for

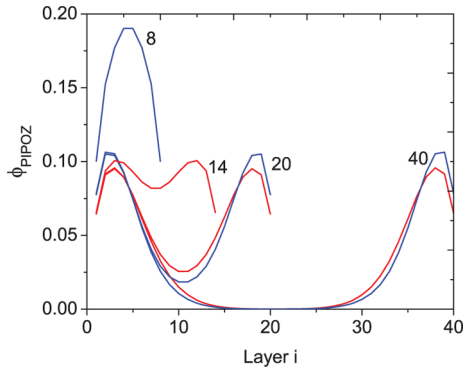

Figure 9. Calculated PIPOZ volume fraction ϕ_{PIPOZ} between two PIPOZ-grafted surfaces as a function of the layer i at surface separation (i) M = 40, (ii) M = 20, and (iii) $M = M_{min}$ at T = 300 K (red) and 325 K (blue) with M_{min} = 14 at T = 300 K and M_{min} = 8 at T = 325 K. The values of the surface separations are indicated.

noninteracting surfaces (M = 40), surfaces at separation M = 20, and surfaces located at their interaction minima. At the separation M = 40, we notice that the polymer volume fraction essentially becomes zero in the middle of the gap, hence motivating the notion of noninteracting polymer layers. Moreover, at the higher temperature the polymer layers are less extended and possesses a higher polymer volume fraction near the surface, in agreement with the PIPOZ segments being more hydrophobic. The difference in the volume fraction profiles at T = 300 and 325 K is modest, due to the relatively low polymer volume fraction. The same theory applied to a similar model system with a polymer possessing r = 1000 segments at the grafting density σ = 0.08, representing an end-grafted PNIPAAM polymer brush, displayed a much larger structural change upon similar temperature increase.[32]

At the intermediate separation M = 20, the outer part of the polymer layer penetrates the other layer. The volume fraction profile of the 6−7 layers closest to the surface remains however unaffected compared to at the larger separation, M = 40 (cf. curves for i = 1 to ca. 8 in Figure 9), and the interaction energy is slightly negative but still close to zero (Figure 7).

At separations corresponding to interaction minima, the volume fraction profiles strongly penetrate each other. At the lower temperature T = 300 K, the two polymer layers can still be distinguished, whereas at T = 325 K, they have merged into a single polymer layer with the maximal volume fraction nearly doubled that of an isolated surface. Thus, the shift to shorter separation of the location of the interaction minimum in the temperature interval T = 300−325 K appears under a coalesene of the two grafted polymer layers into a single one.

The degree of mutual penetration is examined by considering the fraction of polymer segments that penetrates into the other layer as defined in the inset of Figure 10. The fraction of

DOI: 10.1021/la504653w
Langmuir 2015, 31, 3039−3048

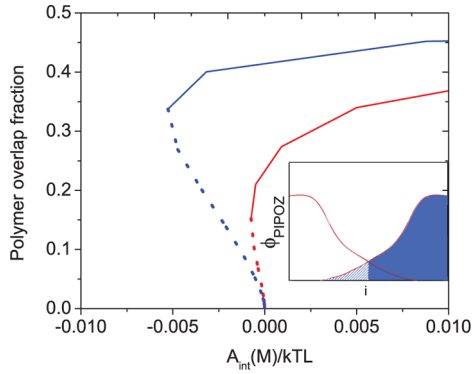

Figure 10. Calculated polymer overlap fraction between two PIPOZ-grafted surfaces as a function of the interaction energy $A_{int}(M)/kTL$ at T = 300 K (red) and T = 325 K (blue) indicated for attractive (dotted curves) and repulsive (solid curves) force branches. The polymer overlap fraction is defined as the fraction of polymer segments (hashed area) penetrating into the polymer layer grafted on the opposite surface (see inset).

penetrating segments as a function of the interaction energy at T = 300 and 325 K are shown in Figure 10. We notice that (i) the fraction of penetrating segments increases with increasing interaction energy on the repulsive branch of the interaction energy curve and (ii) for a given interaction energy the degree of penetration increases with increasing temperature. Hence, converted to the experimental geometry (plane + sphere), for a given force load, our model calculations predict a larger degree of penetration with increasing temperature, i.e., when the polymer layers becomes more hydrophobic. A comparison made at same separation predicts a much smaller difference of the polymer overlap fraction between the two temperatures. That is, however, not the relevant condition at which the friction experiments were performed.

It is commonly stated that the main energy dissipative mechanism operating between polymer-coated surfaces is due to polymer chains being dragged through a region in which polymer chains from both the opposing surfaces reside.[49] Here we show that under static conditions this region increases as the solvent conditions become worse. It seems plausible that the same would be true during sliding, and if so an increased interpenetration region would contribute to the increased friction observed at higher temperatures. However, to clarify the validity of this suggestion will require another modeling approach than that used in the present work.

4. CONCLUSIONS

Normal and friction forces acting between thermoresponsive polymer layers formed on silica surfaces have been investigated as a function of temperature. The layers were prepared by adsorption of a diblock copolymer, poly(2-isopropyl-2-oxazoline)$_{60}$-*b*-poly(3-acrylamidopropylmethylammonium)$_{17}$ (PIPOZ$_{60}$-*b*-PAMPTMA$_{17}$). The cationic block provides strong anchoring to the surface, and the polymer remained on the surface under the highest load applied during shearing, corresponding to a pressure of 33 MPa. The adsorbed amount of PIPOZ$_{60}$-*b*-PAMPTMA$_{17}$ was relatively low, and thus no proper brush layer was formed. The interaction between the layers formed was found to change from purely repulsive at low temperature to partly attractive at higher temperatures due to worsening of the solvent condition. The observed temperature variation in polymer−polymer interaction was reproduced in lattice mean-field calculations. The calculations also show that the segment density distribution between the two PIPOZ coated surfaces changes significantly with temperature at short separations. At low temperatures two segment density maxima are observed, one associated with each layer. In contrast, the two layers merge at higher temperatures, and then only one segment density maximum is found at short separations. We also find that the degree of chain interpenetration under a given load increases with increasing temperature, a finding that we suggest is important for the temperature-dependent friction properties of these layers. Experimentally, we find that the friction force vs load relationship is not well described by Amontons' first law, suggesting that different energy dissipative mechanisms dominate in different load regimes. Generally, the friction force at a given load increases with increasing temperature up to 45 °C, which is a consequence of water progressively becoming a worse solvent for the PIPOZ chain, which also results in increasing chain interpenetration at a given load. However, the friction force at 50 °C was found to be slightly lower than that found at 45 °C, which we suggest is due to the tendency of PIPOZ chains to crystallize in aqueous solutions above the phase separation temperature. Such a crystallization event cannot be captured in the mean-field modeling approach used in this work.

■ ASSOCIATED CONTENT

Supporting Information

Cleaning procedures for substrate, the normal and friction forces measurements, and a brief description of the lattice mean-field theory. This material is available free of charge via the Internet at http://pubs.acs.org.

■ AUTHOR INFORMATION

Corresponding Author

*E-mail: percl@kth.se (P.M.C.).

Notes

The authors declare no competing financial interest.

■ ACKNOWLEDGMENTS

P.C., J.A., and P.L. acknowledge financial support from the Swedish Research Council (VR). X.L. acknowledges a CSC scholarship grant.

■ REFERENCES

(1) Gil, E. S.; Hudson, S. M. Stimuli-Reponsive Polymers and Their Bioconjugates. *Prog. Polym. Sci.* **2004**, *29*, 1173−1222.

(2) Cole, M. A.; Voelcker, N. H.; Thissen, H.; Griesser, H. J. Stimuli-Responsive Interfaces and Systems for the Control of Protein−Surface and Cell−Surface Interactions. *Biomaterials* **2009**, *30*, 1827−1850.

(3) Rzaev, Z. M. O.; Dinçer, S.; Pişkin, E. Functional Copolymers of N-isopropylacrylamide for Bioengineering Applications. *Prog. Polym. Sci.* **2007**, *32*, 534−595.

(4) Alexandridis, P.; Holzwarth, J. F. Differential Scanning Calorimetry Investigation of the Effect of Salts on Aqueous Solution Properties of an Amphiphilic Block Copolymer (Poloxamer). *Langmuir* **1997**, *13*, 6074−6082.

(5) Kawaguchi, S.; Imai, G.; Suzuki, J.; Miyahara, A.; Kitano, T.; Ito, K. Aqueous Solution Properties of Oligo- and Poly(ethylene oxide) by Static Light Scattering and Intrinsic Viscosity. *Polymer* **1997**, *38*, 2885−2891.

(6) Alexandridis, P.; Holzwarth, J. F.; Hatton, T. A. Micellization of Poly(ethylene oxide)-Poly(propylene oxide)-Poly(ethylene oxide) Triblock Copolymers in Aqueous Solutions: Thermodynamics of Copolymer Association. *Macromolecules* **1994**, *27*, 2414−2425.

DOI: 10.1021/la504653w
Langmuir 2015, 31, 3039−3048

(7) Thormann, E. On Understanding of the Hofmeister Effect: How Addition of Salt Alters the Stability of Temperature Responsive Polymers in Aqueous Solutions. *RSC Adv.* **2012**, *2*, 8297−8305.
(8) Nordgren, N.; Rutland, M. W. Tunable Nanolubrication between Dual-Responsive Polyionic Grafts. *Nano Lett.* **2009**, *9*, 2984−2990.
(9) Zhou, L.; Yuan, W.; Yuan, J.; Hong, X. Preparation of Double-Responsive SiO_2-g-PDMAEMA Nanoparticles via ATRP. *Mater. Lett.* **2008**, *62*, 1372−1375.
(10) Korchagina, E. V.; Qiu, X.-P.; Winnik, F. M. Effect of Heating Rate on the Pathway for Vesicle Formation in Salt-Free Aqueous Solutions of Thermosensitive Cationic Diblock Copolymers. *Macromolecules* **2013**, *46*, 2341−2351.
(11) Demirel, A. L.; Meyer, M.; Schlaad, H. Formation of Polyamide Nanofibers by Directional Crystallization in Aqueous Solution. *Angew. Chem., Int. Ed.* **2007**, *46*, 8622−8624.
(12) Lenz, P. Wetting Phenomena on Structured Surfaces. *Adv. Mater.* **1999**, *11*, 1531−1534.
(13) Jones, D. M.; Smith, J. R.; Huck, W. T. S.; Alexander, C. Variable Adhesion of Micropatterned Thermoresponsive Polymer Brushes: AFM Investigations of Poly(N-isopropylacrylamide) Brushes Prepared by Surface-Initiated Polymerizations. *Adv. Mater.* **2002**, *14*, 1130−1134.
(14) Dedinaite, A.; Thormann, E.; Olanya, G.; Claesson, P. M.; Nystrom, B.; Kjoniksen, A.-L.; Zhu, K. Friction in Aqueous Media Tuned by Temperature-Responsive Polymer Layers. *Soft Matter* **2010**, *6*, 2489−2498.
(15) Contreras-García, A.; Alvarez-Lorenzo, C.; Taboada, C.; Concheiro, A.; Bucio, E. Stimuli-Responsive Networks Grafted onto Polypropylene for the Sustained Delivery of Nsaids. *Acta Biomater.* **2011**, *7*, 996−1008.
(16) Arndt, K.-F.; Kuckling, D.; Richter, A. Application of Sensitive Hydrogels in Flow Control. *Polym. Adv. Technol.* **2000**, *11*, 496−505.
(17) Akiyama, Y.; Kikuchi, A.; Yamato, M.; Okano, T. Ultrathin Poly(N-isopropylacrylamide) Grafted Layer on Polystyrene Surfaces for Cell Adhesion/Detachment Control. *Langmuir* **2004**, *20*, 5506−5511.
(18) Schild, H. G. Poly(N-Isopropylacrylamide): Experiment, Theory and Application. *Prog. Polym. Sci.* **1992**, *17*, 163−249.
(19) Erbil, C.; Sezai Saraç, A. Description of the Turbidity Measurements near the Phase Transition Temperature of Poly(N-isopropyl acrylamide) Copolymers: the Effect of pH, Concentration, Hydrophilic and Hydrophobic Content on the Turbidity. *Eur. Polym. J.* **2002**, *38*, 1305−1310.
(20) Cooperstein, M. A.; Canavan, H. E. Biological Cell Detachment from Poly(N-isopropyl acrylamide) and Its Applications. *Langmuir* **2009**, *26*, 7695−7707.
(21) Ionov, L.; Stamm, M.; Diez, S. Reversible Switching of Microtubule Motility Using Thermoresponsive Polymer Surfaces. *Nano Lett.* **2006**, *6*, 1982−1987.
(22) Han, C.-C.; Wei, T.-C.; Wu, C.-S.; Liu, Y.-L. Temperature-Responsive Poly(Tetrafluoroethylene) Membranes Grafted with Branched Poly(N-Isopropylacrylamide) Chains. *J. Membr. Sci.* **2010**, *358*, 60−66.
(23) Konradi, R.; Acikgoz, C.; Textor, M. Polyoxazolines for Nonfouling Surface Coatings — A Direct Comparison to the Gold Standard PEG. *Macromol. Rapid Commun.* **2012**, *33*, 1663−1676.
(24) Hoogenboom, R. Poly(2-oxazoline)s: A Polymer Class with Numerous Potential Applications. *Angew. Chem., Int. Ed.* **2009**, *48*, 7978−7994.
(25) Rehfeldt, F.; Tanaka, M.; Pagnoni, L.; Jordan, R. Static and Dynamic Swelling of Grafted Poly(2-alkyl-2-oxazoline)s. *Langmuir* **2002**, *18*, 4908−4914.
(26) Konradi, R.; Pidhatika, B.; Muhlebach, A.; Textor, M. Poly-2-methyl-2-oxazoline: A Peptide-like Polymer for Protein-Repellent Surfaces. *Langmuir* **2008**, *24*, 613−616.
(27) Agrawal, M.; Rueda, J. C.; Uhlmann, P.; Müller, M.; Simon, F.; Stamm, M. Facile Approach to Grafting of Poly(2-oxazoline) Brushes on Macroscopic Surfaces and Applications Thereof. *ACS Appl. Mater. Interfaces* **2012**, *4*, 1357−1364.
(28) An, J.; Dėdinaitė, A.; Winnik, F. M.; Qiu, X.-P.; Claesson, P. M. Temperature-Dependent Adsorption and Adsorption Hysteresis of a Thermoresponsive Diblock Copolymer. *Langmuir* **2014**, *30*, 4333−4341.
(29) de la Rosa, V. R. Poly(2-oxazoline)s as Materials for Biomedical Applications. *J. Mater. Sci., Mater. Med.* **2014**, *25* (5), 1211−1225.
(30) Shovsky, A.; Knohl, S.; Dedinaite, A.; Zhu, K.; Kjøniksen, A.-L.; Nyström, B.; Linse, P.; Claesson, P. M. Cationic Poly(N-isopropylacrylamide) Block Copolymer Adsorption Investigated by Dual Polarization Interferometry and Lattice Mean-Field Theory. *Langmuir* **2012**, *28*, 14028−14038.
(31) Linse, P.; Claesson, P. M. Modeling of Bottle-Brush Polymer Adsorption onto Mica and Silica Surfaces. *Macromolecules* **2009**, *42*, 6310−6318.
(32) Zhang, J.; Nylander, T.; Campbell, R. A.; Rennie, A. R.; Zauscher, S.; Linse, P. Novel Evaluation Method of Neutron Reflectivity Data Applied to Stimulus-Responsive Polymer Brushes. *Soft Matter* **2008**, *4*, 500−509.
(33) Litt, M.; Rahl, F.; Roldan, L. G. Polymerization of Cyclic Imino Ethers. VI. X-ray Study of Some Polyaziridines. *J. Polym. Sci., Part B: Polym. Phys.* **1969**, *7*, 463−473.
(34) Hoogenboom, R.; Thijs, H. M. L.; Jochems, M. J. H. C.; van Lankvelt, B. M.; Fijten, M. W. M.; Schubert, U. S. Tuning the LCST of Poly(2-oxazoline)s by Varying Composition and Molecular Weight: Alternatives to Poly(N-isopropylacrylamide)? *Chem. Commun.* **2008**, 5758−5760.
(35) Katsumoto, Y.; Tsuchiizu, A.; Qiu, X.; Winnik, F. M. Dissecting the Mechanism of the Heat-Induced Phase Separation and Crystallization of Poly(2-isopropyl-2-oxazoline) in Water through Vibrational Spectroscopy and Molecular Orbital Calculations. *Macromolecules* **2012**, *45*, 3531−3541.
(36) Green, C. P.; Lioe, H.; Cleveland, J. P.; Proksch, R.; Mulvaney, P.; Sader, J. E. Normal and Torsional Spring Constants of Atomic Force Microscope Cantilevers. *Rev. Sci. Instrum.* **2004**, *75*, 1988−1996.
(37) Sader, J. E.; Chon, J. W. M.; Mulvaney, P. Calibration of Rectangular Atomic Force Microscope Cantilevers. *Rev. Sci. Instrum.* **1999**, *70*, 3967−3969.
(38) Pettersson, T.; Nordgren, N.; Rutland, M. W.; Feiler, A. Comparison of Different Methods to Calibrate Torsional Spring Constant and Photodetector for Atomic Force Microscopy Friction Measurements in Air and Liquid. *Rev. Sci. Instrum.* **2007**, *78*.
(39) Liu, X.; Dedinaite, A.; Nylander, T.; Dabkowska, A. P.; Skoda, M.; Makuska, R.; Claesson, P. M. Association of Anionic Surfactant and Physisorbed Branched Brush Layers Probed by Neutron and Optical Reflectometry. *J. Colloid Interface Sci.* **2015**, *440*, 245−252.
(40) Scheutjens, J. M. H. M.; Fleer, G. J. Statistical Theory of the Adsorption of Interacting Chain Molecules. 1. Partition Function, Segment Density Distribution, and Adsorption Isotherms. *J. Phys. Chem.* **1979**, *83*, 1619−1635.
(41) Fleer, G. J.; Stuart, M. A. C.; Scheutjens, J. M. H. M.; Cosgrove, T.; Vincent, B. *Polymers at Interfaces*; Chapman and Hall: London, 1993; p 496.
(42) Linse, P.; Bjoerling, M. Lattice Theory for Multicomponent Mixtures of Copolymers with Internal Degrees of Freedom in Heterogeneous Systems. *Macromolecules* **1991**, *24*, 6700−6711.
(43) Karlstroem, G. A New Model for Upper and Lower Critical Solution Temperatures in Poly(ethylene oxide) Solutions. *J. Phys. Chem.* **1985**, *89*, 4962−4964.
(44) Malmsten, M.; Linse, P.; Zhang, K. W. Phase Behavior of Aqueous Poly(ethylene oxide)/Poly(propylene oxide) Solutions. *Macromolecules* **1993**, *26*, 2905−2910.
(45) Zhao, J.; Hoogenboom, R.; Van Assche, G.; Van Mele, B. Demixing and Remixing Kinetics of Poly(2-isopropyl-2-oxazoline) (PIPOZ) Aqueous Solutions Studied by Modulated Temperature Differential Scanning Calorimetry. *Macromolecules* **2010**, *43*, 6853−6860.
(46) Claesson, P. M.; Kjellander, R.; Stenius, P.; Christenson, H. K. Direct Measurement of Temperature-Dependent Interactions between

DOI: 10.1021/la504653w
Langmuir 2015, 31, 3039−3048

Non-ionic Surfactant Layers. *J. Chem. Soc., Faraday Trans. 1* **1986**, *82*, 2735−2746.
(47) Malmsten, M.; Claesson, P. M.; Pezron, E.; Pezron, I. Temperature-Dependent Forces between Hydrophobic Surfaces Coated with Ethyl Hydroxyethyl Cellulose. *Langmuir* **1990**, *6*, 1572−1578.
(48) Malmsten, M.; Claesson, P. M. Temperature-Dependent Adsorption and Surface Forces in Aqueous Ethyl(hydroxyethyl)-Cellulose Solutions. *Langmuir* **1991**, *7*, 988−994.
(49) Raviv, U.; Tadmor, R.; Klein, J. Shear and Frictional Interactions between Adsorbed Polymer Layers in a Good Solvent. *J. Phys. Chem. B* **2001**, *105*, 8125−8134.
(50) Klein, J. Shear, Friction, and Lubrication Forces Between Polymer-Bearing Surfaces. *Annu. Rev. Mater. Sci.* **1996**, *26*, 581−612.
(51) Yoshizawa, H.; Chen, Y. L.; Israelachvili, J. Fundamental Mechanisms of Interfacial Friction. 1. Relation Between Adhesion and Friction. *J. Phys. Chem.* **1993**, *97*, 4128−4140.
(52) Johnson, K. L.; Kendall, K.; Roberts, A. D. Surface Energy and the Contact of Elastic Solids. *Proc. R. Soc. London, Ser. A* **1971**, *324*, 301−313.

DOI: 10.1021/la504653w
Langmuir 2015, 31, 3039−3048